


Probabilistic Learning for Decision-making on Civil Infrastructures | Published: 12 March 2018

A Probabilistic Safety Evaluation Framework for Multi-Hazard Assessment in a Bridge using SO-MARS Learning Model

[Kuo-Wei Liao](#) , [Nhat-Duc Hoang](#) & [Jessica Gitomarsono](#)

[KSCE Journal of Civil Engineering](#) **22**, 903–915(2018) | [Cite this article](#)

140 Accesses | **4** Citations

A Probabilistic Safety Evaluation Framework for Multi-Hazard Assessment in a Bridge using SO-MARS Learning Model

Kuo-Wei Liao*, Nhat-Duc Hoang**, and Jessica Gitommarsono***

Received August 31, 2017/Revised November 7, 2017/Accepted November 25, 2017/Published Online

Abstract

A probabilistic evaluation procedure is established to assess a bridge safety against floods and earthquakes, which are the two major threats of a bridge in Taiwan. Scour depth distribution is used to reflect the flood hazard, in which swarm optimized multivariate adaptive regression splines (SO-MARS) is utilized to calculate scour depth density followed by Monte Carlo Simulation (MCS) and a scour risk curve is constructed. Displacement ductility is used to measure the bridge performance under attacks of both hazards through nonlinear time history analyses followed by a power law regression to build the fragility curve. A code-based probabilistic seismic hazard curve is constructed and the joint failure probability under seismic and flood attacks is obtained. A numerical example is provided to illustrate the proposed methodology, in which the nonlinear behaviors in concrete (including core and cover areas), steel bar and soil are included in a bridge model. A threshold scour depth for a given earthquake (e.g., the return period or the peak ground acceleration is given) is derived to meet a specified target reliability. The suggested scour depth is a deterministic number which is immediately applicable in engineering practice.

Keywords: *reliability, multi-hazard, flood, seismic, bridge safety, SO-MARS*

1. Introduction

Due to frequent earthquakes in Taiwan, the concept of aseismic design has been treated significantly by engineers, and the corresponding regulations are also relatively complete. However, with global climate changes, natural calamities are occurring frequently around the globe. In addition, the global greenhouse effect has also caused the gradual increase of the frequency of natural calamities of abnormal weather, typhoons, floods, etc. as well as the magnitude of loss associated therewith. Under the attacks of multiple disasters, the possibility of damage or collapse of bridges also increases. In this paper, a bridge safety analysis process with the consideration of earthquakes and flood scouring is established, in which uncertainties of parameters, such as scour depth, are incorporated in to the calculations.

The safety of a river-crossing bridge is often affected by the level of scouring at the pier foundation. Melville and Coleman (2000) defined that the common river scouring mechanisms can be divided into three types: general scouring (long-term degradation scour), contraction scouring and local scouring. Degradation scour refers to the lowering or scouring of the streambed over relatively long reaches due to a deficit in sediment supply from upstream and contributes to total scour (Richardson and Davis, 2001), wherein the latter two types occur due to the existence of

the pier foundation. Specifically, Contraction scour is a lowering of the streambed across the stream or waterway bed at the bridge and local scour refers to removal of material from around piers, abutments, spurs, and embankments (Richardson and Davis, 2001). The local scouring has the most significant impact on the bridge structure. In the past, many scholars have proposed prediction equations for local scour depth. For example, equations proposed by HEC-18 (US Department of Transportation, 2012) and Melville & Coleman (2000) are broadly used to consider the non-uniform pier structures commonly seen in Taiwan. HEC-18 uses the concept of the superposition method to calculate the maximum scour depth at a non-uniform pier. Taking a pile group foundation for an example, in the HEC-18 method, the bridge foundation is divided into three parts of the pier stem, pile cap and pile group. The scour depth component of each part is calculated individually, followed by addition to obtain the prediction value. On the other hand, Melville and Raudkivi (1996) introduced the concept of an equivalent uniform pier width conversion using the width of the original pier, river depth, and river bed elevation. Such method is able to effectively simplify the non-uniform pier into a uniform pier in order to calculate the local scour depth. Melville and Coleman (2000) proposed to calculate the uniform pier local scour depth by multiplying several empiric correction parameters including the categories of the pier foundation shape

*Associate Professor, Dept. of Bioenvironmental Systems Engineering, National Taiwan University, 1, Section 4, Roosevelt Road, Taipei, Taiwan (Corresponding Author, E-mail: kliao@ntu.edu.tw)

**Lecturer, Faculty of Civil Engineering, Institute of Research and Development, Duy Tan University (E-mail: hoangnhatduc@dtu.edu.vn)

***Former Graduate Student, No. 43, Keelung Rd., Sec.4, Da'an Dist., Taipei 10607, Taiwan (E-mail: jessica.gitommarsono@gmail.com)

and dimension, water flow velocity, sediment dimension, angle of attack of water flow, river channel shape, time factor, etc.

In addition to the previous two approaches, machine learning is another approach that can be utilized to build the scour prediction model. For example, a quadratic polynomial of Group Method of Data Handling (GMDH) network, improved by the back propagation algorithm, is proposed to predict scour depth around bridge piers (Najafzadeh and Azamathulla, 2013). With their promising results, the Multivariate Adaptive Regression Splines (MARS) originally proposed by Friedman (1991) is incorporated with Firefly Algorithm (FA) to predict the local scour depth in the current study. 174 experimental data entries, including different pier sizes, flow depths and soil covering depths, are collected to build the MARS model. In constructing the predicting model, MARS divides the high-dimensional learning space into sub-ranges for influencing variables and establishes a mapping relationship between the influencing variables and the target parameter using piecewise linear function (Friedman, 1991; Parsaie *et al.*, 2016). MARS is a generalization of stepwise linear regression or a variant of regression tree with capability to provide a promising prediction model. Notably, the approach of MARS is based on a divide-and-conquer strategy within the historical data separated into distinctive regions; in which each data is provided with a regression line (Goh *et al.*, 2017). Therefore, MARS is highly suitable for modeling complex engineering data. On the other hand, the model establishment of MARS requires a proper setting of two tuning parameters: the maximum number of *BFs* (k_{max}) and the penalty coefficient (c). Previous works have demonstrated that the determination of tuning parameters necessitates great efforts (Hoang *et al.*, 2017; Zhang *et al.*, 2015; Koc *et al.*, 2015). Moreover, since the penalty coefficient is searched in a continuous domain, the results of conventional method (e.g. grid search) may not be optimal. Accordingly, an integration of MARS and the Firefly Algorithm (FA) is adopted in the current study. FA, as a metaheuristic method, is employed to search for an appropriate set of tuning parameters (k_{max} and c) that features the highest model accuracy. Once the MARS-based model is built, Monte Carlo simulation (MCS) with the hydraulic data is used to generate scour depths and a scour hazard is constructed.

A probabilistic seismic hazard curve, built by Probabilistic Seismic Hazard Analysis (PSHA), is used to evaluate the seismic hazard for the investigated river bridge. The PSHA is to evaluate the hazard of seismic ground motion at a site by considering all possible earthquakes in the area, estimating the associated shaking at the site, and calculating the probabilities of these occurrences (McGuire, 2004). Cornell (1968) assumed that an earthquake was a point earthquake source, the occurrence of an earthquake event followed the Poisson Process and the earthquake scale distribution followed the Gutenberg–Richter recurrence law. The PSHA used in the engineering fields nowadays is mostly derived from the analysis procedure proposed by Cornell (1968). Kiureghian and Ang (1977) proposed the fault-rupture model by correcting the drawback of underestimation of analysis result due

to the use of a point earthquake source in the Cornell method. Schwartz and Coppersmith (Schwartz, 1984; Youngs, 1985) proposed the “Characteristic Earthquake Model” by using the fault slip velocity to establish the relationship between the recurrence rate and the earthquake scale. Although the seismic hazard is important, developing a new seismic hazard model is beyond the scope of the current study. Instead, the model built from National Center for Research on Earthquake Engineering (NCREE) is commonly accepted in Taiwan and therefore, is adopted here. For details, please refer to Jean (2017). Based on their model, a seismic hazard curve at a location at the investigated bridge is built.

To illustrate the proposed methodology, a numerical example is provided. SAP2000 is used to model the investigated bridge. To consider the nonlinear behavior of the substructure, a nonlinear link element is used to simulate the behavior of a predefined plastic hinge calculated using Xtract, in which the constitutive laws of core concrete, cover concrete and steel bar are included. The soil behavior is simulated by a series of depth-dependent soil springs around the caisson. The stiffness/coefficient of soil spring varies significantly for different empirical equations. A code-based formula based on the standard penetration test is used to calculate the soil property. Details of the proposed methodology is provided below

2. The Proposed Method

Using fragility curve to measure bridge performance under multi-hazard threats has gained increasing attention in recent years (Wang *et al.*, 2012; Ganesh Prasad and Banerjee, 2013; Dong *et al.*, 2013; Kim *et al.*, 2017). Wang *et al.* (2012) indicated that the occurrence of scour depth increases potential risk of plastic hinge formulation on the pile head due to the dynamic effect of the pile cap. To consider the scour hazard, Ganesh Prasad and Banerjee (2013) used the HEC-18 to calculate the local scour depth. In addition, to reduce the cost of structural analysis, their bridge foundation is simulated using an equivalent single pile. Dong *et al.* (2013) considered structural deterioration in their flood-induced seismic evaluation and bridge performance is described in terms of sustainability. Kim *et al.* (2017) focused on establishing the flood fragility of bridges, in which reliability analysis is performed in conjunction with finite element analysis. Compared to previous studies, this study establishes a frame to evaluate a bridge performance using fragility curve, in which several aspects are innovative and are different from those of previous studies. For example, a machine learning algorithm, swarm optimized multivariate adaptive regression splines (SO-MARS), is developed to calculate the local scour depth. In addition, the bridge foundation is not simplified and the effect of the pile group on scour depth can be included. The details are described below.

To establish the fragility curve and the joint probability distribution function under multiple disasters, the proposed process is displayed in Fig. 1. First, the relevant information, including the

situated location, soil characteristics and hydraulic condition, etc. of the bridge site is obtained. In addition, the structural configuration information of the example bridge is obtained, including the detailed content of the structure construction drawings, cross sectional dimensions, material characteristics, detailed designs, etc. Next, the aforementioned information is used to calculate the structural cross sectional property of the bridge substructures (pier and caisson) in order to obtain the structural nonlinear property. The substructure plastic hinge property is calculated according to the failure mode (flexural, shear or combined model). The soil nonlinear elastic model is established according to the soil information. Seven earthquake records are collected and their response spectrums are scaled to fit the design response spectrum. To be specific, for a damping ratio of 5%, the response spectrum of the selected earthquakes falling in between 0.2 T and 1.5 T as the fundamental period) may not be lower than 90% of the corresponding design spectral acceleration. In addition, the mean value of the response spectrum within the designated period range may not be lower than the average value of the corresponding design spectral accelerations. Nonlinear time history analysis is performed with the scaled ground motions. Based on the analysis results, a fragility curve is established by using the displacement ductility as an index. Together with the occurrence probabilities of the seismic hazard level and scouring hazard, the joint probability distribution function is calculated. Please note that the probability of the simultaneous occurrence of two extreme events (i.e., scour and earthquake) is generally small. Three models for considering the combination effects of extreme loads using reliability approaches are often adopted in practical applications. They are: (1) Turkstra's rule, (2) the Ferry

Borges-Castanheta model, and (3) Wen's load coincidence method (Ghosn *et al.*, 2003). Many researchers have made great efforts on investigating the load combination effect. It is very unusual to find scour occurs that follow earthquakes in Taiwan. This study investigated the safety performance of a scoured bridge under seismic excitations. Thus, this study considers the occurrence probabilities of scour and earthquake events to be statistically independent in calculating their combination effects using simulation approach. In view of the above, nonlinear plastic hinge property, flood scouring hazard level and fragility analysis are the main focuses of this research, which are described in details as follows.

3. Failure Mode Analysis of Plastic Hinge

The design parameters obtained are used to define the plastic hinge properties in the bridge numerical model in order to simulate the non-linear behavior of the bridge structure under nonlinear time history analysis. The failure mode analysis of piers proposed by Sung (2005) is adopted and it can be divided into three types: shear failure, flexural to shear failure and flexural failure. The moment capacity of the pier or caisson can be analyzed from the flexure and shear behaviors of the cross section and the result can be compared in order to determine which of the two (flexure or shear) dominates. The flexural behavior analysis uses the cross section analysis software, Xtract, to establish the relationship ($M_b - \phi$) between the moment and curvature in order to further obtain the relationship between the moment and angle ($M_b - \theta$ Model). The resultant internal couple in a cross-section of the structural element is referred to the "moment" and the "curvature" is the quotient of the longitudinal strain for a given point and its distance to the neutral axis. The shear behavior analysis uses the recommendation of the Taiwan Seismic Design Specifications for Highway and Bridges to calculate the shear strength, and it is converted into the relationship between moment and angle ($M_v - \theta$ Model) in order to perform stacking comparison with the $M_b - \theta$ Model, such that the pier moment capacity is obtained. The plastic hinges are arranged at four areas of the pier bottom, depth of 4 m, 8 m and 10 m under the river bed.

As mentioned above, the relationship between the moment and curvature of the cross section is established by using the Xtract software, such as M_y , ϕ_y and M_u , ϕ_u . For the corresponding displacement and angle, assuming that the pier bottom end is a fixed end, the elastic displacement (δ) at the top end of the pier can be expressed as

$$\delta = \int_0^h \phi_i y_i dy \quad (1)$$

where h refers to the column height, and y_i refers to the distance downward from the column top when the cross section curvature is ϕ_i . Its corresponding equivalent angle is

$$\theta = \frac{\delta}{h} \quad (2)$$

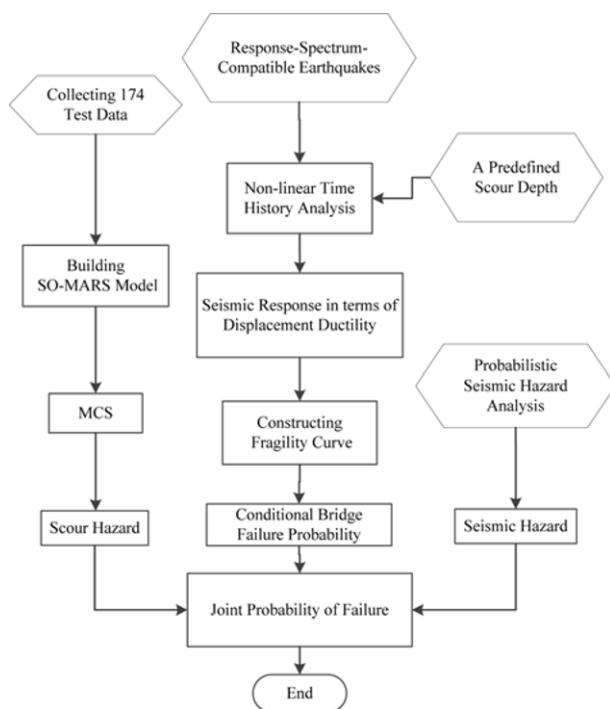


Fig. 1. The Flowchart of This Research

Assuming that when the pier is under an elastic state, the curvature φ_i and the distance y_i away from the column top is of a linear relationship; therefore, the curvature φ_i under the yield state is

$$\varphi_i = \frac{y_i}{h} \varphi_y \quad (3)$$

where φ_y refers to the crack curvature or yield curvature. Yield displacement δ_y can be expressed as

$$\delta_y = \int_0^h \frac{y_i}{h} \varphi_y y_i dy = \frac{\varphi_y h^2}{3} \quad (4)$$

Equivalent yield angle θ_y is

$$\theta_y = \frac{\delta_y}{h} \quad (5)$$

Plastic displacement (δ_p) is

$$\delta_p = \int_{h-L_p}^h (\varphi_u - \varphi_y) y_i dy = (\varphi_u - \varphi_y) L_p \left(h - \frac{L_p}{2} \right) \quad (6)$$

where L_p refers to the equivalent plastic hinge length, and the definition from Paulay and Priestley (1992) is used here as follows

$$L_p = 0.08h + 0.022d_{bl}\sigma_y \quad (7)$$

where d_{bl} refers to the longitudinal steel bar diameter, and σ_y refers to the steel bar yield stress. Equivalent ultimate angle θ_u is

$$\theta_u = \frac{\delta_y}{h} + \frac{\delta_p}{h - \frac{L_p}{2}} \quad (8)$$

After obtaining θ_y and θ_u , along with the M_y and M_u , an $M_b - \theta$ model can be established.

The pier shear strength calculation method is based on the Taiwan Seismic Design Specifications for Highway and Bridges, and the methods proposed by Priestley (1994) and Aschheim (1992) are adopted as shown in the following.

$$V_c = 0.53(k + F) \sqrt{\frac{100}{9.81} f'_c (MPa) \times 0.01 A_g (mm^2)} \times 9.81 (N) \quad (9)$$

where k refers to the rotation ductility factor, which equals 1 before flexural yielding and decreases linearly to zero at the flexural ultimate condition; F is the axial load effect on the shear strength, which equals $N/(13.8A_g)$ (MPa) for a compressive axial load and $N/(3.5A_g)$ (MPa) for a tensile axial load, where N is the axial force and A_g is the gross cross-sectional area; A_e is the effective area, which equals $0.8 A_g$. To consider the concrete contribution in shear strength, the cover and core areas of the concrete are calculated separately, followed by adding the values together, the concrete shear strength equation is calculated by Eq. (10).

$$V_c = V_{c,core} + V_{c,cover} \quad (10)$$

In addition, the lateral steel bar shear strength of circular cross section can be expressed as

$$V_s = \frac{A_{sh} f_y d \alpha}{s} \quad (11)$$

where A_{sh} is the area of the shear reinforcement; d is the effective sectional depth; s is the vertical spacing; and $\alpha = 1$ for a rectangular section and $\pi/2$ for a circular section.

Therefore, the normal shear strength V_n of the column can be obtained as

$$V_n = V_c + V_s \quad (12)$$

Furthermore, the pier normal shear strength can be viewed as the function $V_n(\theta)$ of the angle, and when yield has not yet occurred:

$$V_n(\theta \leq \theta_y) = V_c + V_s \quad (13)$$

Under ultimate limit state:

$$V_n(\theta = \theta_u) = V_s \quad (14)$$

According to Song's suggestion (2005), the shear strength value between the yield state and the ultimate limit state can be obtained from linear interpolation:

When yield not yet occurs ($\theta \leq \theta_y$)

$$M_{vy} = V_n(\theta_y) \times h \quad (15)$$

Under ultimate limit state ($\theta = \theta_u$)

$$M_{vu} = V_n(\theta_u) \times \left(h - \frac{L_p}{2} \right) \quad (16)$$

During non-elastic section ($\theta_y \leq \theta \leq \theta_u$) is

$$M_v = M_{vy} + (M_{vu} - M_{vy}) \times \frac{R - 1}{R_{max} - 1} \quad (17)$$

According to the above method, a relationship graph ($M_v - \theta$ Model) between shear converted moment and angle can be

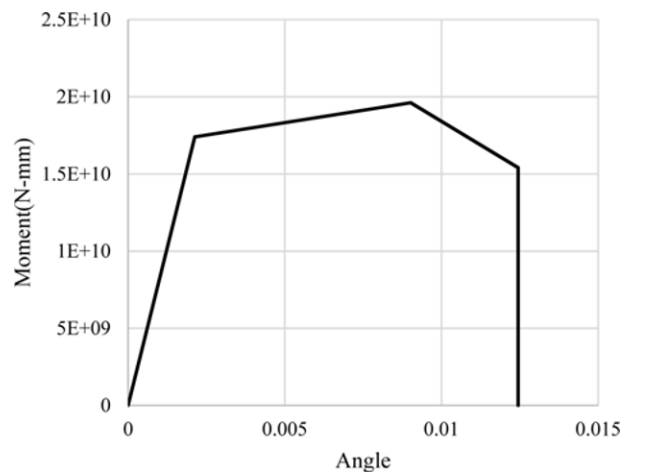


Fig. 2. Example of Moment and Angle Model at a Pier Bottom of the Demonstrated Bridge

established. Three possible failure modes are described in brief as follows: (1) When the shear converted yield moment is less than the flexure yield moment ($M_{vy} < M_{by}$), it is considered as the shear failure mode. (2) When the shear converted yield moment is higher than the flexure yield moment ($M_{vy} > M_{by}$), and when the non-elastic section shear converted moment is lower than the flexure moment ($M_v < M_b$), it is considered as the flexure-shear failure mode. (3) When the flexure moment capacity is always smaller than the shear converted moment ($M_b < M_v$), it is considered as the flexure failure mode. Fig. 2 is an example that shows the relationship between the moment and angle of a pier in the pier bottom of the investigated bridge.

4. Flood Scouring Hazard Level Analysis

The calculation of scour depth in this study is based on the proposed SO-MARS which is described in details as shown below. Please note that the pier-group effect (Akib *et al.*, 2014) is not considered and only one-dimension hydraulic analysis is included in the current study. Further validation is needed to generalize the use of current finding in future applications, especially, when effects of the pier-group and river cross section are significant.

5. Description of MARS

MARS (Friedman, 1991) is a novel method for constructing modeling equations from the collecting data. This method divides the high-dimensional learning space into several sub-ranges of the prediction variables to establish a mapping relationship between the prediction variables and the targeted output variable (Parsaie *et al.*, 2016). MARS uses a piecewise linear function for fitting each local model and employs an adaptive approach to finalize model. Evidences of MARS as a powerful machine learning tool are observed in plentiful previous studies (Cheng and Cao, 2016). MARS-based model is expressed through a series of simple basis functions (*BFs*) which characterize the relationship between input and output variables. A *BF* is shown as follows:

$$b_m(x) = \max(0, C - x) \text{ or } b_m(x) = \max(0, x - C) \quad (18)$$

where b_m denotes a *BF*; x is an input variable; C represents a threshold parameter used to divide the original range of x into sub-ranges.

The general form of the MARS model is expressed as follows:

$$f(x) = \alpha_0 + \sum_{m=1}^k \alpha_m b_m(x) \quad (19)$$

where $\alpha_0, \alpha_1, \dots, \alpha_M$ are weighting coefficients; $f(x)$ represents the model output. k denotes the number of weighting coefficients. The model establishment of MARS is broken down into two steps: forward and backward steps. In the first step, *BFs* are added into the model so that they can help to reduce the training error; this process is terminated when the maximum number of

BF is reached. The second step is to alleviate overfitting phenomenon by pruning redundant *BFs*. Each sub-model of MARS is evaluated by the generalized cross-validation (GCV) index (Jekabsons, 2016; Suman *et al.*, 2016) as shown in Eq. (20).

$$GCV = MSE / (1 - \frac{k + 0.5c(k-1)}{n})^2 \quad (20)$$

where MSE stands for mean square error of the model, k denotes the number of *BFs*. n represents the number of observations in the training data. c is a penalty coefficient; Friedman (1991) and Jekabsons (2016) recommend that this parameter should be searched within the range of [2, 4].

6. Firefly Algorithm (FA)

In order to commence the training process of MARS, two tuning parameters, namely the maximum number of *BFs* (k_{max}) and the penalty coefficient (c), are required to be determined. A proper setting of these tuning parameters is necessary to achieve a desirable performance of the MARS model. Thus, in this study, FA (Yang, 2008; Yang, 2010) is utilized as a means for tuning the model free parameters. The description of FA is provided below.

Often, the pattern of firefly flashes is unique for a particular species. In essence, each firefly is attracted to brighter ones as it randomly explores while searching for prey. Based on the nature phenomenon, FA is formulated as a global optimization method which is an advanced swarm intelligence that can effectively locate the optimum. Superior performance of FA has been demonstrated in previous research works (Cheng and Hoang, 2017; Tilahun *et al.*, 2017). The FA method utilizes the following rules: (1) all fireflies are unisex, so each firefly is attracted to other fireflies regardless of their sex, (2) the attractiveness of a firefly is proportional to its brightness and decreases as the distance increases. A firefly moves randomly if no other firefly is brighter, and (3) the brightness of a firefly is affected or determined by the landscape of the objective function. The FA pseudo code is illustrated in Fig. 3.

The brightness of an individual firefly can be defined similarly

```

Begin FA
Define the cost function  $f(x)$ , where  $x=(x_1, \dots, x_d)$ 
Generate an initial population of fireflies
Formulate the light intensity  $I$ 
Define the absorption coefficient  $\gamma_L$ 
While ( $t < \text{Max\_Generation}$ )
  For  $i = 1$  to  $n$  (all  $n$  fireflies)
    For  $j = 1$  to  $n$  (all  $n$  fireflies)
      If ( $I_j > I_i$ ), move firefly  $i$  towards firefly  $j$ 
    End if
    Evaluate new solutions and update light intensity;
  End for  $j$ 
  End for  $i$ 
  Rank the fireflies and find the current best
   $t = t + 1$ 
End while
End FA

```

Fig. 3. The FA Pseudo Code

to the fitness value in the genetic algorithm. The light intensity $I(r)$ varies according to the following equation:

$$I(r) = I_o \exp(-\gamma_L r^2) \quad (21)$$

where I_o denotes the light intensity of the source. γ_L is the light absorption coefficient. r represents the distance from the source.

As the attractiveness of a firefly is proportional to the light intensity seen by adjacent fireflies, the attractiveness β of a firefly is defined as:

$$\beta = \beta_o \exp(-\gamma_L r^2) \quad (22)$$

In a D -dimensional space, the distance between any two fireflies i at x_i and j at x_j , is calculated as follows:

$$r_{ij} = \|x_i - x_j\| = \sqrt{\sum_{k=1}^D (x_{i,k} - x_{j,k})^2} \quad (23)$$

Since a specific firefly x_i is attracted to the brighter one x_j , the movement of the i^{th} firefly can be expressed as:

$$x_i = x_i + \beta_o \exp(-\gamma_L r_{ij}^2) (x_j - x_i) + \alpha(\omega - 0.5) \quad (24)$$

where γ_L is the light absorption coefficient, γ_L varies from 0.1 to 10; β_o represents the attractiveness at $r_{ij} = 0$; α denotes a trade-off constant to determine the random behavior of movement; ω represents a random number drawn from the Gaussian distribution.

7. The Proposed SO-MARS Model for Evaluating Scour Depth

The establishment of the proposed SO-MARS model is accomplished by a fusion of MARS and FA. The model flow

chart is illustrated in Fig. 4. The SO-MARS employs MARS as the supervised learning algorithm for learning the implicit functional relationship between the input features and the scour depth. Furthermore, the FA swarm intelligence method is utilized to automatically identify the optimal values of the MARS's tuning parameters.

Before the model training and prediction phases, a preliminary analysis on variable relevancy is performed to identify irrelevant input variables. In this study, the ReliefF method (Robnik-Šikonja and Kononenko, 2003) is utilized to compute the independence relationship of each conditioning variable to the output variable (i.e., scour depth). ReliefF is capable of detecting conditional dependencies between attributes and provides a unified view on the attribute relevancy in regression problems (Robnik-Šikonja and Kononenko, 1997). This method assigns a weight value for each input variable that expresses its importance; the higher the weight, the more relevant the input variable.

Before performing FA, initial values of the aforementioned tuning parameters (denoted as k_{max} and c) are randomly generated within the range of lower and upper bounds in the following manner:

$$X_{i,0} = LB + \text{rand}[0,1] \times (UB - LB) \quad (25)$$

where $X_{i,0}$ is the tuning parameter i at the first generation. $\text{rand}[0,1]$ denotes a uniformly distributed random number between 0 and 1. LB and UB are two vectors of lower and upper bounds for parameters which are 5 and 50, respectively; bounds for the parameter c are 0.1 and 4.

During the searching process, the FA automatically explores the various combinations of the tuning parameters (k_{max} and c). At each generation, the fitness of each individual combination is

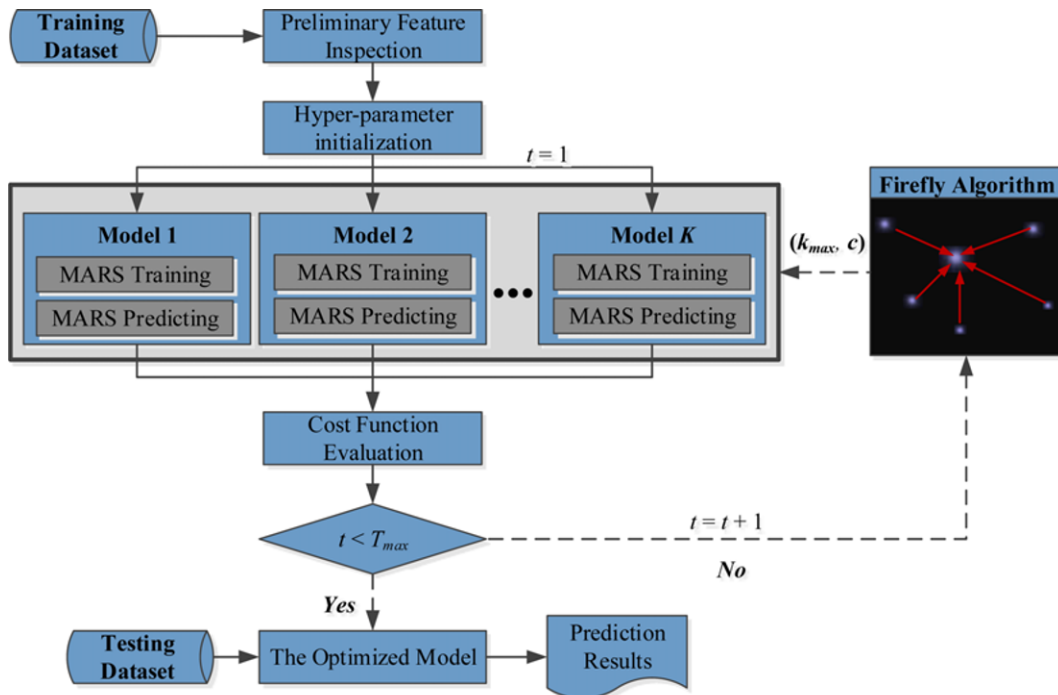


Fig. 4. The Proposed SO-MARS Model

evaluated and the optimizer discards inferior combinations, and allows robust combinations to be passed on the next generations. Through such process, the optimal solution can be found. Furthermore, in order to determine the optimal set of tuning parameters, the training data set is divided into K exclusive folds. Generally, a larger number of data folds deliver a better set of the model's tuning parameters. However, the computational cost can be very high for adopting SO-MARS as a hybrid machine learning model. Thus, it is reasonable to select a value of K that can sufficiently determine the appropriate model parameters within an acceptable computational expense. Herein, based on the size of the collected data set and the suggestions of previous works (Arlot, 2010; Breiman *et al.*, 1984; Cheng and Hoang, 2014), K is selected to be 5. In each run, a data fold is used as a validating set and the other folds are employed for model training. The robustness of each parameter set is appraised via the average performance of the K validating data folds. A prediction model built based on this strategy is often with a good generalization capability. Accordingly, the following objective function is used for cost function evaluation:

$$F_{\text{cost}} = \frac{\sum_{i=1}^K E_i^{VA}}{K} \quad (26)$$

In Eq. (26), E_i^{VA} denotes the validating error of the i^{th} data fold. The employed validating error is Root Mean Squared Error (RMSE). FA will not terminate unless the maximum number of generation is achieved. Once terminates, an optimized set of tuning parameters can be identified which means the SO-MARS model is established and is ready to carry out prediction phase.

8. Experimental Results of SO-MARS Based Scour Depth Prediction

This study collects 174 data samples of clear-water scour in

Table 1. Description of Data for Scour Depth Prediction

Influencing factor	Notation	Unit	Min	Average	Std.	Max
IF ₁	y	m	0.13	0.22	0.12	0.60
IF ₂	b_c	m	0.01	0.04	0.03	0.15
IF ₃	b_{pc}	m	0.05	0.10	0.06	0.37
IF ₄	L_u	m	0.01	0.13	0.41	2.78
IF ₅	Y	m	-0.67	-0.02	0.12	0.21
IF ₆	V/V_c	-	0.53	0.89	0.13	1.18
IF ₇	d_{50}	mm	0.06	0.62	0.22	1.00
IF ₈	σ_g	-	1.00	1.12	0.12	1.30
Y	d_s	m	0.01	0.09	0.05	0.34

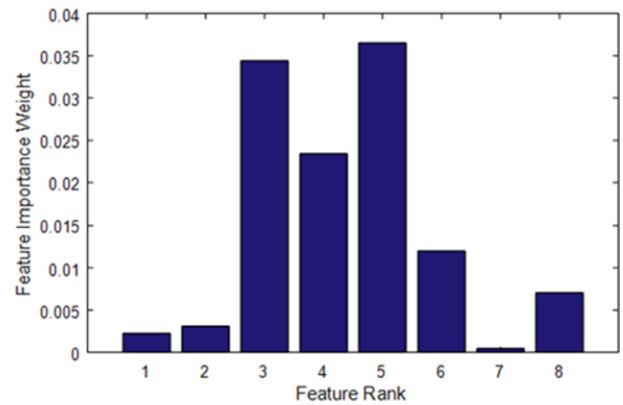


Fig. 5. Feature ranking with ReliefF

which 170 of them are from previous experimental works (Ataie-Ashtiani *et al.*, 2010; Melville and Raudkivi, 1996) and 4 of them are testing results conducted in the Hydrotech Research Institute of the National Taiwan University. The 8 influencing factors, including the flow depth y , the pier width perpendicular to the flow direction b_c , the pile-cap width b_{pc} , the longitudinal extension of pile cap face out from pier face L_u , the soil covering

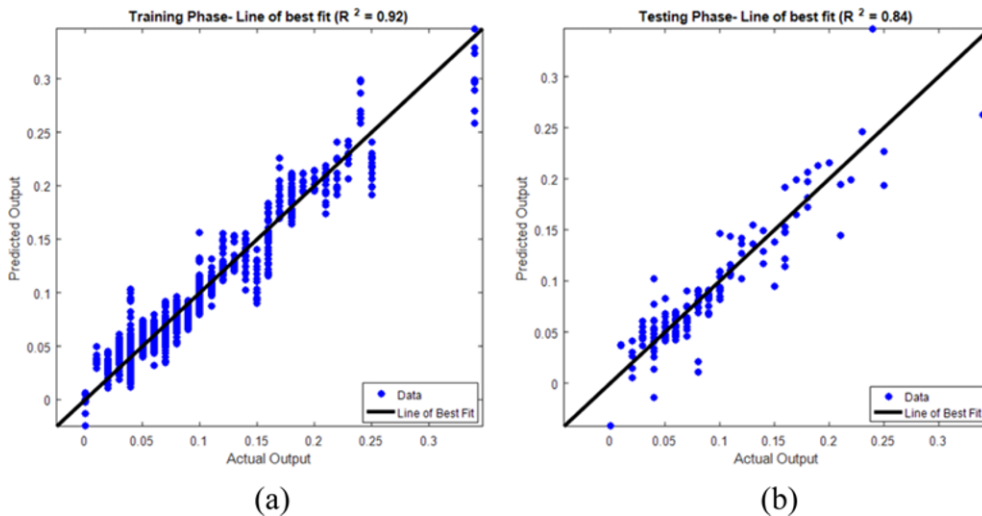


Fig. 6. Results of the Ten-fold Cross Validation Process: (a) Training Phase: RMSE = 0.016 (0.001) and $R^2 = 0.92$ (0.001), (b) Testing Phase: RMSE = 0.022 (0.006) and $R^2 = 0.84$ (0.001)

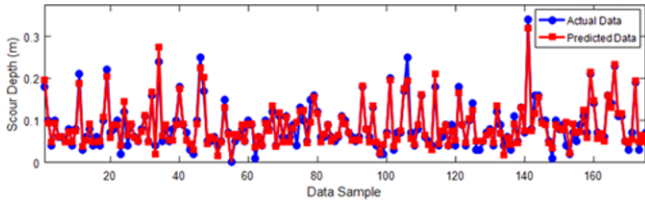


Fig. 7. Results of SO-MARS Trained with the Whole Data Set

height Y , the ratio of the mean velocity to the critical velocity of sediment movement V/V_c , the median grain size d_{50} , and the river bed material geometric standard deviation σ_g , are employed to estimate the scour depth d_s of complex pier foundations. The statistical descriptions of all variables are provided in Table 1.

A preliminary investigation, the ReliefF (Robnik-Šikonja and Kononenko, 2003), on the relevancy of each conditioning variable is employed here and the analysis result is shown in Fig. 5. It is shown that IF_5 is the most influential factor, followed by IF_3 , IF_4 , and IF_6 . The variables IF_8 , IF_2 , IF_1 , and IF_7 demonstrate moderate and minor relevancy. Nevertheless, because none of the weight values are null, indicating that all factors are relevant for characterizing the scour depth.

The average values of k_{\max} and c obtained from the ten-fold cross validation process are 24.26 and 2.61, respectively (Fig. 6). Therefore, the parameters of $k_{\max} = 25$ and $c = 2.61$ are employed to retrain the MARS model with the whole historical data set. The model accuracy is desirable with $RMSE = 0.015$ and $R^2 = 0.93$. The model prediction result is graphically illustrated in Fig. 7. The MARS-based scour depth prediction model is shown as follows:

$$Y = 0.205 - 4.82 \times BF_1 + 0.21 \times BF_2 - 0.812 \times BF_3 + 211 \times BF_4 + 12.8 \times BF_5 - 10.90 \times BF_6 + 4.89 \times BF_7 + 2.83 \times BF_8 - 0.236 \times BF_9 + 14.9 \times BF_{10} - 83.80 \times BF_{11} - 93.80 \times BF_{12} - 3.01 \times BF_{13} + 2.35 \times BF_{14} - 1.79 \times BF_{15} - 3.87 \times BF_{16}$$

where

Y denotes the output variable of scour depth. IF_i represents the i th influencing factor. The detailed BF is shown as follows:

$$\begin{aligned} BF_1 &= \max(0, IF_2 - 0.10) \\ BF_2 &= \max(0, IF_4 - 0.05) \\ BF_3 &= \max(0, 0.33 - IF_1) \\ BF_4 &= \max(0, 0.33 - IF_1) \times \max(0, IF_5 + 0.16) \times \max(0, IF_6 - 1.00) \\ BF_5 &= \max(0, 0.33 - IF_1) \times \max(0, IF_5 + 0.16) \times \max(0, 10 - IF_6) \\ BF_6 &= \max(0, 0.10 - IF_2) \times \max(0, IF_5 + 0.16) \\ BF_7 &= \max(0, 0.10 - IF_2) \times \max(0, -0.16 - IF_5) \\ BF_8 &= \max(0, IF_5 + 0.06) \\ BF_9 &= \max(0, -0.06 - IF_5) \\ BF_{10} &= \max(0, 0.10 - IF_2) \times \max(0, IF_5 - 0.03) \\ BF_{11} &= \max(0, 0.1 - IF_2) \times \max(0, 0.03 - IF_5) \times \max(0, IF_3 - 0.08) \\ BF_{12} &= \max(0, 0.10 - IF_2) \times \max(0, 0.03 - IF_5) \times \max(0, 0.08 - IF_3) \\ BF_{13} &= \max(0, IF_5 + 0.05) \\ BF_{14} &= BF_3 \times \max(0, IF_6 - 0.74) \\ BF_{15} &= BF_3 \times \max(0, 0.74 - IF_6) \\ BF_{16} &= BF_8 \times \max(0, IF_4 - 0.07) \end{aligned}$$

It is noted that although results of ReliefF indicate that all

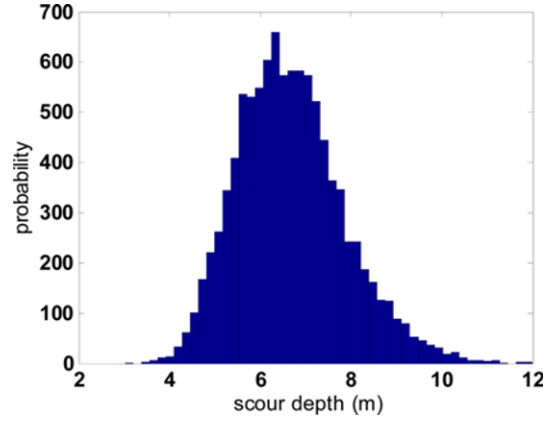


Fig. 8. Histogram of the Occurrence Number of Scour Depth Based on SO-MARS Model

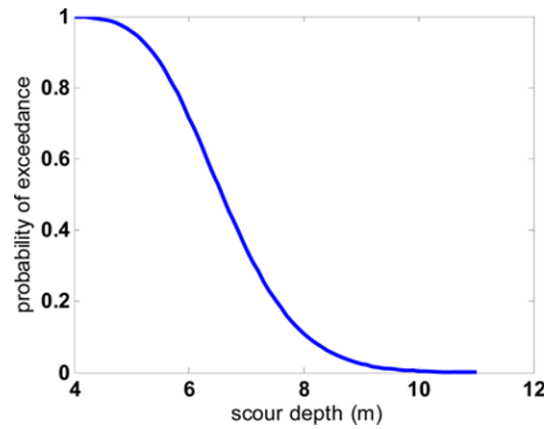


Fig. 9. SO-MARS Based Risk Curve of Scour Depth at the Investigated Bridge

influencing factors should be employed. MARS has cast out the IF_7 and IF_8 from the final prediction model which is reasonable because IF_7 and IF_8 are used to distinguish the clear water and live bed scours and all the collected data are generated from the clear water condition, these two factors do not have significant impact on the scour depth. To obtain the probability distribution of scour depth, an MCS with a sample size of 10^6 is used to establish the distribution curve of the scour depth and exceedance probability, as shown in Figs. 8 and 9, in which the water depth and water velocity are reproduced via LN (1.60, 0.13) and LN (0.70, 0.34), respectively (Liao *et al.*, 2015).

9. Ground Motions, Seismic Hazard and Fragility Curve

Based on results of a series of nonlinear time-history analyses, a fragility curve can be constructed as described below. Based on recommendation of the Load and Resistance Factor Design (LRFD) seismic bridge design of the American Association of State Highway and Transportation Officials (AASHTO) guide specification (AASHTO, 2007), seven ground motions are selected from the Pacific Earthquake Engineering Research

Table 2. Details of the Selected Ground Motions

Ground Motion	Year	Station	Magnitude	Distance (km)	Mechanism
San Fernando	1971	LA - Hollywood	6.61	22.77	Reverse
Imperial Valley	1979	El Centro	6.53	19.76	Strike Slip
Loma Prieta	1989	Corralitos	6.93	0.16	Reverse Oblique
Northridge	1994	Glendale – Las Palmas	6.69	21.64	Reverse
Kobe	1995	Kakogawa	6.90	22.50	Strike Slip
Chi-Chi (TCU52)	1999	TCU 052	6.20	58.86	Strike Slip
Chi-Chi (TCU68)	1999	TCU 068	6.20	67.56	Strike Slip

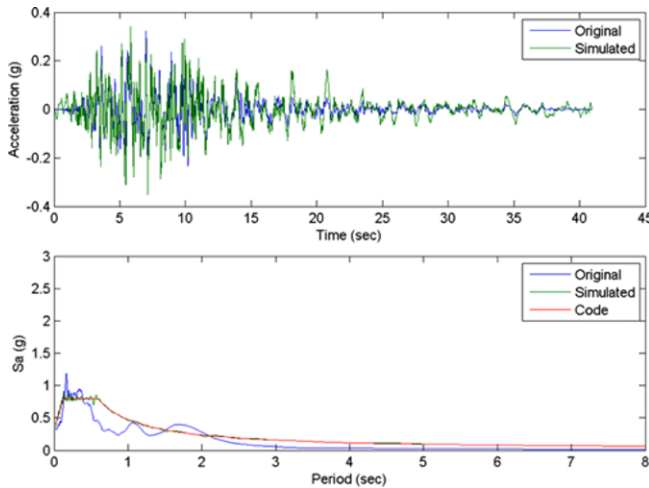


Fig. 10. Example of Kobe-Kakogawa Earthquake and Scaled Spectrum Compatible with the Design Spectrum of 475 years

Ground Motion Database (PEER). The details of the selected ground motions are described in Table 2.

The selected ground motions are further scaled to “response-spectrum-compatible” records. To be specific, a response-spectrum-compatible time history refers to the response spectrum of the selected earthquakes falling in between 0.2 T and 1.5 T is the fundamental period); however, it may not be less than 90% of the corresponding design spectral acceleration for a damping ratio of 5%. In addition, the average value of the response spectrum within the designated period range may not be less than the average value of the corresponding design spectral accelerations. The ground motions used in this study are converted into response-spectrum-compatible data for return periods of 30, 475, and 2500 years, as shown in Fig. 10. In addition to the ground motions with this three return periods, ground motions with Peak Ground Acceleration (PGA) of 1.0 and 1.5 g are also included in our time history analysis as indicated in Table 3.

The bridge safety against two hazards is investigated through a probabilistic approach in this study. The flood hazard is represented by the aforementioned probabilistic scour curve (Fig. 9). The PSHA is used to measure the seismic risk. Based on Jean’s approach (2017), a seismic hazard curve at the investigated bridge is built, as shown in Fig. 11. The displacement ductility (D_Δ), defined as the ratio of the displacement of the bridge girder

Table 3. Summary of Time-history Analyses Conducted in This Study

Earthquake	PGA (Return period)	Scour depth	Total No.
San Fernando	0.091 (30 years)		
Imperial Valley	0.363 (475 years)	4 m	
Loma Prieta	0.453 (2500 years)	8 m	
Northridge	1.007	10 m	
Kobe	1.510		
Chi-Chi (TCU52)			
Chi-Chi (TCU68)			
			105

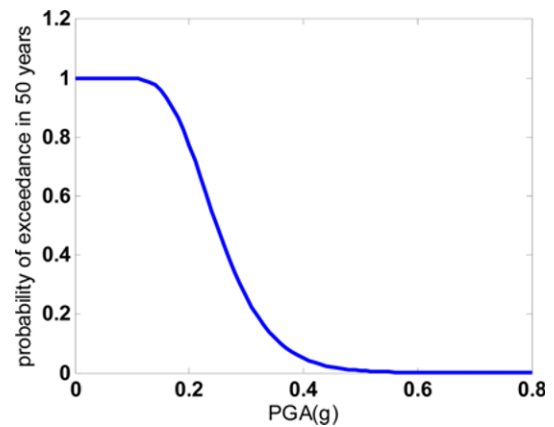


Fig. 11. Seismic Hazard Curve for Investigated Bridge

to the yield displacement of a pier, is used to measure the structural performance under seismic excitations. To build a relationship between PGA and μ_Δ , a regression using the power law equation is performed as indicated in Eq. (27).

$$D_\Delta = a(PGA)^b \quad (27)$$

where a and b are regression constants. For a given PGA, if both capacity and demand follow log-normally distribution, the failure probability is computed as described in Eq. (28) known as a fragility curve.

$$P_f(\mu_\Delta > \mu | PGA = x) = 1 - \Phi \left(\frac{\ln \left(\frac{\mu}{D_\Delta} \right)}{\sigma_{\mu_\Delta | PGA}} \right) \quad (28)$$

in which μ is the mean capacity (Alipour *et al.*, 2013), D_Δ is the mean demand converted from PGA, σ is the standard deviation for a given o the limit state, and Φ is the cumulative probability

density function of the standard normal. The capacity of the displacement ductility for varied limit states are $1 < \mu < 2$, $2 < \mu < 4$, $4 < \mu < 7$, $\mu > 7$ for slight, moderate, major, and complete collapse damages, respectively (Alipour *et al.*, 2013). For a given PGA, the standard deviation ($\sigma_{\mu_s|PGA}$) is calculated using Eq. (29).

$$\sigma_{\mu_s|PGA} = \sqrt{\sigma_{D|PGA}^2 + \sigma_c^2} \quad (29)$$

where $\sigma_{D|PGA}$ is the standard deviation of the demand for a given PGA, and σ_c is the standard deviation of the capacity (i.e., 0.5) (NCEE, 2009). $\sigma_{D|PGA}$ is obtained by performing another regression analysis as indicated in Eq. (30).

$$\sigma_{D|PGA} = c(PGA)^f \quad (30)$$

10. Result and Discussion

The pier 14 (P14), pier 15 (P15) and the superstructure between these two piers of Nanyun Bridge are selected to demonstrate the proposed methodology, as shown in Fig. 12. The selected bridge has 23 spans in the road direction and its total length is around



Fig. 12. The Bridge Investigated in This Study

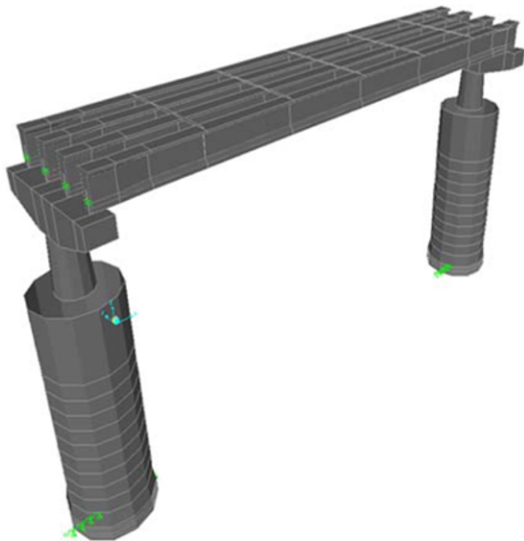


Fig. 13. The Finite Element Model of the Bridge Investigated in This Study

920 m with an equal span length of 40 m. The width of this bridge is 10 m. As shown, a single pier with a caisson foundation is used. The length of P14 and P15 is 7.6 m. Two concrete strengths, 28 MPa and 21 MPa, are used for the bridge pier and caisson, respectively. When diameter of steel bar less than or equal to 16 mm, the SD280 is used. SD420W is used for diameters greater than 16 mm. The finite element model is shown in Fig. 13. Assuming that the bridge deck possesses infinite in-plane stiffness and a rigid body constraint is used to simulate such behavior. The fundamental frequency of the built numerical model is 3.28 Hz which is close to the on-site measurement of 3.04 Hz.

When a bridge is subject to withstanding the i th number of river scouring event (SC_i) and the j th number of earthquake event (EQ_j), the failure probability for the damage state (DS_k) is

$$(P_f)_{ijk} = P(SC_i \cap EQ_j \cap DS_k) \quad (31)$$

In general, the failure probability for the damage state (DS_k) is calculated using Eq. (32). Because scouring and earthquakes are both low-probability high-consequence events, it is reasonable to assume that the statistics of scouring and earthquake events are independent from each other; therefore, the above joint probability can be expressed as

$$(P_f)_{ijk} = P(DS_k | SC_i EQ_j) \times P(EQ_j, SC_i) \quad (32)$$

$$(P_f)_{ijk} = P(SC_i) P(EQ_j) P(DS_k) \quad (33)$$

where $P(SC_i)$ refers to the probability of occurrence of a given scour depth (i), which can be obtained from the scouring hazard analysis; $P(EQ_j)$ refers to the probability of occurrence of certain PGA (j), which can be obtained from PSHA; $P(DS_k)$ refers to the exceedance probability of the bridge exceeding a certain performance level (k), which can be obtained from time history analyses.

After performing nonlinear time history analysis under varied scour depths, the corresponding structure displacement ductility performance for each set of external seismic excitations can be obtained. Results of the above time-history analyses only provide failure probabilities at five different PGA values. To build a fragility curve, a continuous failure-probability function in terms of PGA is required. For this reason, with the mean displacement ductility values and standard deviations analyzed from seven entries of data in each set, regression analysis is further performed, and the a, b, c, and f described in Eqs. (27) and (30) are obtained as shown in Table 4.

A fragility curve can be generated based on Table 4. Fig. 14 shows the fragility curves under slight-, moderate- and major-damage states for a bridge with scour depths of 4, 8, and 10 m,

Table 4. Regression Results for Mean and Standard Deviation of Displacement Ductility for Scour Depths of 4, 8, and 10 m

Scour Depth (m)	Constant			
	a	b	c	f
4	3.80	1.04	0.46	1.53
8	4.40	1.05	0.60	1.51
10	5.48	1.01	0.65	1.25

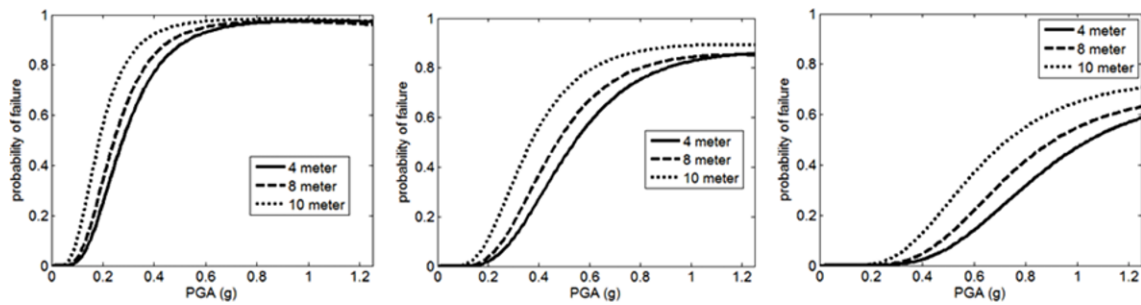


Fig. 14. Fragility Curves with Different Scour Depths Under Slight-, Moderate- and Major-damage States (left, middle and right)

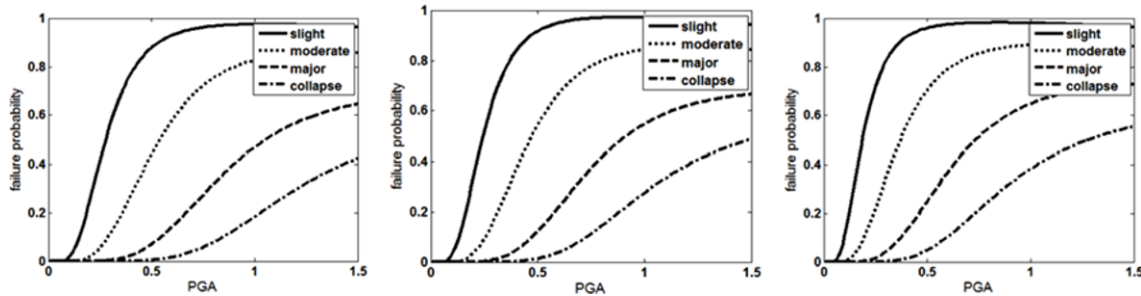


Fig. 15. Fragility Curves with Different Damage States Under 4, 8, and 10 meters (left, middle and right)

respectively. Two things are observed: First, the failure probability increases with the increase in the scour depth. Second, the failure probability decreases as the limit state changes from slight to collapse. In addition, it is found that the failure probability is not proportional to the increase of the scour depth. As shown, the failure probability increases dramatically as the scour depth changes from 8 to 10 m for both limit states. Alternatively, fragility curves with different damage states under each scour depth (i.e., 4, 8, and 10 meters) are displayed in Fig. 15.

Based on Eq. (33), the joint-failure probabilities are developed within a scour depth range of 4 m to 10 m. Interpolation is utilized for scour depth between 4 m and 10 m. Extrapolation is not conducted when the scour depth is outside the range of 4 m and 10 m due to it often fails to provide a satisfied fitting. Figs. 16-18 show the joint probability of failure for slight-, moderate- and major-damage states, respectively.

It is understood that the proposed methodology is too complicated to be adopted in engineering practice. It is also known that due to frequent earthquakes in Taiwan, the concept of aseismic design has been treated significantly by engineers, and the corresponding regulations are relatively complete. Thus, this study calculates a threshold value for scour depth based on the obtained joint failure probability. That is, when a bridge with the threshold scour depth is confirmed to be safe based on the current seismic regulations, such bridge will survive against both hazards (floods and seismic). To illustrate the above concept, taking the investigated bridge as an example, the design PGA of this Bridge is 0.36 g. If the target of reliability index (β) is set to be 3, the threshold scour depth can be derived, which is approximately equal to 5.5 m as indicated in Fig. 19. That is, engineers can follow their routine design process and if the safety of a bridge with a scour depth of 5.5 m is confirmed, the reliability of such bridges against floods

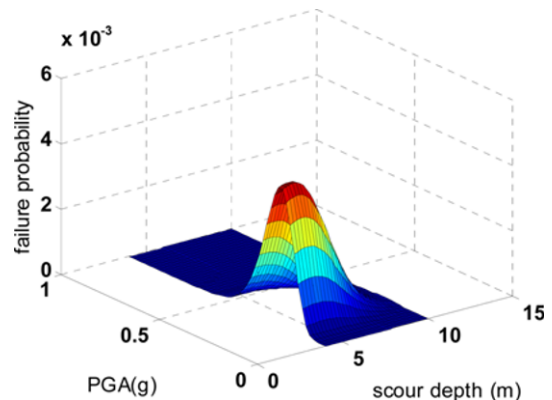


Fig. 16. Joint Probability of Failure for Slight-damage State at the Investigated Bridge

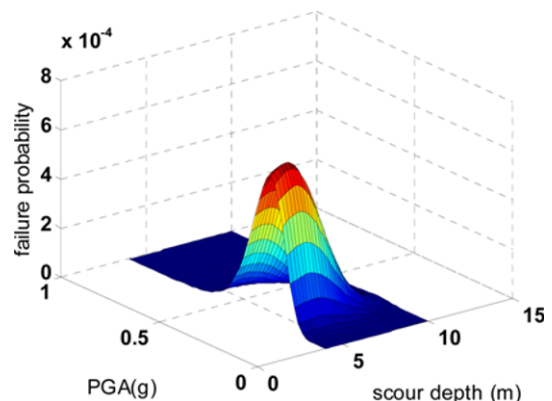


Fig. 17. Joint Probability of Failure for Moderate-damage State at the Investigated Bridge

and earthquakes is ensured at a reliability level of 0.99865 for a moderate-damage state. Note that the probability for scour depth

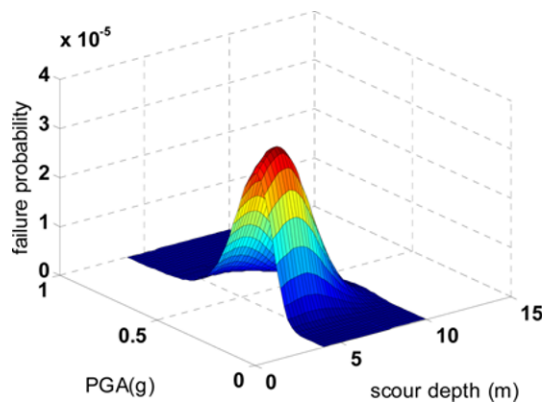


Fig. 18. Joint Probability of Failure for Major-damage State at the Investigated Bridge

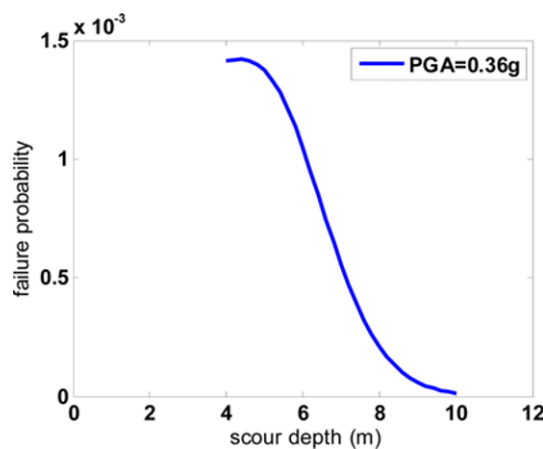


Fig. 19. Joint Failure Probability of the Investigated Bridge for Moderate-damage State at Design PGA

less than 5.5 m is around 0.17 as indicated in Fig. 9. When the seismic hazard is also included, the bridge reliability is 0.99865 which is quite different from 0.17, indicating that the probability of having both hazards is very low. Another possible reason is that the investigated bridge possesses sufficient strength against the considered floods and earthquakes.

11. Conclusions

This study investigates bridge safety against floods and earthquakes, in which uncertainties in many important influencing factors are considered. For example, to measure the scour depth effect, SO-MARS learning algorithm is proposed, in which an optimization algorithm (i.e., FA) is utilized to find the optimal parameters in MARS. With a promising learning performance (e.g., the RMSE and R^2 of the built model are 0.015 and 0.93, respectively), the SO-MARS is incorporated with MCS to describe the scour hazard. In addition, uncertainties in structural response under seismic excitations are considered through time history analyses, in which nonlinear behaviors in core concrete, cover concrete and steel bar are considered to formulate the plastic hinge property. From above calculations, bridge fragility

curve and joint failure probability are established. It is found that for the investigated bridge, it is likely to experience a flood scour with a depth in the range of 4–10 m with mean value and standard deviation of 6.67 and 1.19, respectively. Scour has a significant effect on bridge safety. Taking the moderate-damage state for example, when scour depth increases from 4 m to 10 m, the bridge failure probability increases from 0.08 to 0.4 accordingly. Further, the influence of scour on bridge safety is nonlinear. Based on the calculations, the failure probability does not significantly increase when the scour depth increases from 4 m to 8 m. However, the failure probability considerably changes when the scour depth increases from 8 m to 10 m. To alleviate the design burden in engineering practice, this study calculates a threshold value for scour depth based on the obtained joint failure probability. If the safety of a bridge with the threshold scour depth is confirmed based on the current seismic regulations, this bridge will survive against floods and earthquakes for a given damage state. Based on the obtained threshold value (e.g., 5.5 m), it is known that the strength of the investigated bridge is adequate and the probability of having both hazards in the considered area is very low.

Acknowledgements

This study was supported by the Ministry of Science and Technology of Taiwan under grant number MOST 105-2221-E-011-010-MY3. The support is gratefully acknowledged.

References

- Achheim, M. and Moehle, J. P. (1992). "Shear strength and deformability of reinforced concrete bridge columns Subjected to Inelastic Cyclic Displacements." *College of Engineering University of California at Berkeley*.
- Akib, S., Jahangirzadeh, A., and Basser, H. (2014). "Local scour around complex pier groups and combined piles at semi-integral bridge." *Journal of Hydrology and Hydromechanics*, Vol. 62, No. 2, pp. 108–116, DOI: 10.2478/johh-2014-0015.
- Alipour, A., Shafei, B., and Shinozuka, M. (2013). "Reliability-based calibration of load and resistance factors for design of RC bridges under multiple extreme events: Scour and earthquake." *Journal of Bridge Engineering*, Vol. 18, No. 5, pp. 362–371, DOI: 10.1061/(ASCE)BE.1943-5592.0000369.
- Arlot, S. (2010). "A survey of cross-validation procedures for model selection." *Statistics Surveys*, Vol. 4, pp. 40–79, DOI: 10.1214/09-SS054.
- Arneson, L. A., Zevenbergen, L. W., Lagasse, P. F., and Clopper, P. E. (2012). "Evaluating scour at bridges." *Publication No. 18. FHWA HIF 12-003*, Federal Highway Administration, Washington, D.C.
- Ataie-Ashtiani, B., Baratian-Ghorgchi, Z., and Beheshti, A. A. (2010). "Experimental investigation of clear-water local scour of compound piers." *Journal of Hydraulic Engineering*, Vol. 136, No. 6, pp. 343–351, DOI: 10.1061/(ASCE)0733-9429(2010)136:6(343).
- Azamathulla, H. M., Haghiabi, A. H., and Parsaie, A. (2016). "Prediction of side weir discharge coefficient by support vector machine technique." *Water Science and Technology: Water Supply*, Vol. 16, No. 4, pp. 1002–1016, DOI: 10.2166/ws.2016.014.
- Breiman, L., Friedman, J., Stone, C. J., and Olshen, R. A. (1984). *Classification and Regression Trees*, Chapman and Hall Ltd/CRC,

- New York.
- Cheng, M. Y. and Cao, M. T. (2016). "Estimating strength of rubberized concrete using evolutionary multivariate adaptive regression splines." *J. Civ. Eng. Manag.*, Vol. 22, No. 5, pp. 711-720, DOI: 10.3846/13923730.2014.897989.
- Cheng, M. Y. and Hoang, N. D. (2014). "Groutability prediction of microfine cement based soil improvement using evolutionary LS-SVM Inference model." *J. Civ. Eng. Manag.*, Vol. 20, pp. 1-10, DOI: 10.3846/13923730.2013.802717.
- Cheng, M. Y. and Hoang, N. D. (2017). "Estimating construction duration of diaphragm wall using firefly-tuned least squares support vector machine." *Neural Comput. Appl.*, First Online, DOI: 10.1007/s00521-017-2840-z.
- Cornell, C. A. (1968). "Engineering seismic risk analysis." *Bulletin of the Seismological Society of America*, Vol. 58, No. 5, pp. 1583-1606.
- Der Kiureghian, A. and Ang, A. H-S. (1977). "A fault-rupture model for seismic risk analysis." *Bulletin of the Seismological Society of America*, Vol. 67, No. 4, pp. 1173-1194.
- Dong, Y., Frangopol, D. M., and Saydam, D. (2013). "Time-variant sustainability assessment of seismically vulnerable bridges subjected to multiple hazards." *Earthquake Engineering & Structural Dynamics*, Vol. 42, No. 10, pp. 1451-1467, DOI: 10.1002/eqe.2281.
- Friedman, J. H. (1991). "Multivariate adaptive regression splines." *Ann. Statist.*, Vol. 19, No. 1, pp. 1-67, DOI: 10.1214/aos/1176347963.
- Ganesh Prasad, G. and Banerjee, S. (2013). "The impact of flood-induced scour on seismic fragility characteristics of bridges." *Journal of Earthquake Engineering*, Vol. 17, No. 6, pp. 803-828, DOI: 10.1080/13632469.2013.771593.
- Ghosn, M., Moses, F., and Wang, J. (2003). *Design of highway bridges for extreme events*, Report No. 489, Transportation Research Board, Washington, D.C.
- Goh, A. T. C., Zhang, Y., Zhang, R., Zhang, W., and Xiao, Y. (2017). "Evaluating stability of underground entry-type excavations using multivariate adaptive regression splines and logistic regression." *Tunnelling and Underground Space Technology*, Vol. 70, pp. 148-154, DOI: 10.1016/j.tust.2017.07.013.
- Hoang, N. D., Chen, C. T., and Liao, K. W. (2017). "Prediction of chloride diffusion in cement mortar using multi-gene genetic programming and multivariate adaptive regression splines." *Measurement*, Vol. 112, pp. 141-149, DOI: 10.1016/j.measurement.2017.08.031.
- Jean, W. Y. (2017). "Seismic hazard curves of taiwan and disaster simulation technology." *NCREE report*, Taipei.
- Jekabsons, G. (2016). "ARESLab: Adaptive regression splines toolbox for Matlab/Octave." *Technical report*, Riga Technical University, available at <http://www.cs.rtu.lv/jekabsons/>.
- Kartal Koc, E. and Bozdogan, H. (2015). "Model selection in Multivariate Adaptive Regression Splines (MARS) Using information complexity as the fitness function." *Mach. Learn.*, Vol. 101, pp. 35-58, DOI: 10.1007/S10994-014-5440-5.
- Kim, H., Sim, S. H., Lee, J., Lee, Y. J., and Kim, J. M. (2017). "Flood fragility analysis for bridges with multiple failure modes." *Advances in Mechanical Engineering*, Vol. 9, No. 3, pp. 1-11, DOI: 10.1177/1687814017696415.
- Liao, K. W., Lu, H. J., and Wang, C. Y. (2015). "A probabilistic evaluation of pier-scour potential in the gaoping river basin of Taiwan." *J. Civ. Eng. Manag.*, Vol. 21, pp. 637-653, DOI: 10.3846/13923730.2014.890650.
- McGuire, R. K. (2004). *Seismic hazard and risk analysis*, Earthquake Engineering Research Institute, California, United States.
- Melville, B. W. and Coleman, S. E. (2000). *Bridge scour*, Water Resources Publications, Littleton, Colorado.
- Melville, B. W. and Raudkivi, A. J. (1996). "Effects of foundation geometry on bridge pier scour." *Journal of Hydraulic Engineering*, Vol. 122, No. 4, pp. 203-209, DOI: 10.1061/(ASCE)0733-9429(1996)122:4(203).
- Najafzadeh, M. and Azamathulla, H. M. (2013). "Group method of data handling to predict scour depth around bridge piers." *Neural Computing & Applications*, Vol. 23, Nos. 7-8, pp. 2107-2112, DOI: 10.1007/s00521-012-1160-6.
- Parsaie, A., Haghiabi, A. H., Saneie, M., and Torabi, H. (2016). "Prediction of energy dissipation on the stepped spillway using the multivariate adaptive regression splines." *ISH J. Hydraul. Eng.*, Vol. 22, No. 3, pp. 281-292, DOI: 10.1080/09715010.2016.1201782.
- Paulay, T. and Priestley, M. J. N. (1992). *Seismic design of reinforced concrete and masonry buildings*, John Wiley & Sons, Inc. Newjersey.
- Priestley, M. J. N., Verma, R., and Xiao, Y. (1994). "Seismic shear strength of reinforced concrete columns." *Journal of Structural Engineering*, Vol. 120, No. 8, pp. 2310-2329, DOI: 10.1061/(ASCE)0733-9445(1994)120:8(2310).
- Richardson, E. V. and Davis, S. M. (2001). *Evaluating scour at bridges*, Publication No. FHWA/NHI 01-001, Hydraulic Engineering Circular (HEC) No. 18, Federal Highway Administration, U.S. Department of Transportation, Washington, D.C.
- Robnik-Šikonja, M. and Kononenko, I. (1997). "An adaptation of Relief for attribute estimation in regression." *Machine Learning: Proceedings of the Fourteenth International Conference (ICML 97)*, Morgan Kaufmann., pp. 296-304.
- Robnik-Šikonja, M. and Kononenko, I. (2003). "Theoretical and Empirical Analysis of ReliefF and RReliefF." *Mach. Learn.*, Vol. 53, No. 1, pp. 23-69, DOI: 10.1023/A:1025667309714.
- Schwartz, D. P. and Coppersmith, K. J. (1984). "Fault behavior and characteristic earthquakes: Examples from the wasatch and san andreas fault zones." *Journal of Geophysical Research*, Vol. 89, No. B7, pp. 5681-5698.
- Suman, S., Das, S. K., and Mohanty, R. (2016). "Prediction of friction capacity of driven piles in clay using artificial intelligence techniques." *International Journal of Geotechnical Engineering*, Vol. 10, No. 5, pp. 469-475, DOI: 10.1080/19386362.2016.1169009.
- Sung, Y. C., Liu, K. Y., Su, C. K., Tsai, I. C., and Chang, K. C. (2005). "A study on pushover analyses of reinforced concrete columns." *Structural Engineering and Mechanics*, Vol. 21, No. 1, pp. 35-52, DOI: 10.12989/sem.2005.21.1.035.
- Tilahun, S. L., Ngnotchouye, J. M. T., and Hamadneh, N. N. (2017). "Continuous versions of firefly algorithm: A review." *Artif Intell Rev.*, DOI: 10.1007/s10462-017-9568-0.
- Wang, Z., Song, W., and Li, T. (2012). "Combined fragility surface analysis of earthquake and scour hazards for bridge." *In Proceedings of the 15th World conference on Earthquake Engineering*, pp. 24-28.
- Yang, X. S. (2008). *Firefly algorithm*, Luniver Press, Bristol, UK.
- Yang, X. S. (2010). "Firefly algorithm, stochastic test functions and design optimisation." *Int. J. Bio-inspired Computation*, Vol. 2, No. 2, pp. 78-84, DOI: 10.1504/IJBIC.2010.032124.
- Youngs, R. R. and Coppersmith, K. L. (1985). "Implications of fault slip rates and earthquake recurrence models to probabilistic seismic hazard estimates." *Bulletin of the Seismological Society of America*, Vol. 75, No. 4, pp. 930-964.
- Zhang, W., Goh, A. T. C., Zhang, Y., Chen, Y., and Xiao, Y. (2015). "Assessment of soil liquefaction based on capacity energy concept and multivariate adaptive regression splines." *Eng. Geol.*, Vol. 188, pp. 29-37, DOI: 10.1016/j.enggeo.2015.01.009.